CONTINUUM MECHANICS BASED BI-LINEAR SHEAR DEFORMABLE SHELL ELEMENT USING ABSOLUTE NODAL COORDINATE FORMULATION

Hiroki Yamashita
Department of Mechanical and Industrial Engineering
The University of Iowa
2312 Seamans Center
Iowa City, IA 52242

Antti I. Valkeapää
Department of Mechanical Engineering
Lappeenranta University of Technology
Skinnarilankatu 34,
53850 Lappeenranta, Finland

Paramsothy Jayakumar
US Army RDECOM TARDEC
6501 E. 11 Mile Road
Warren, MI 48397-5000

Hiroyuki Sugiyama
Department of Mechanical and Industrial Engineering
The University of Iowa
2416C Seamans Center
Iowa City, IA 52242
hiroyuki-sugiyama@uiowa.edu

Report Documentation Page

Form Approved
OMB No. 0704-0188

1. REPORT DATE	2. REPORT TYPE	3. DATES COVERED
07 MAR 2014	**Technical Report**	**07-01-2014 to 04-03-2014**

4. TITLE AND SUBTITLE	5a. CONTRACT NUMBER
CONTINUUM MECHANICS BASED BI-LINEAR SHEAR DEFORMABLE SHELL ELEMENT USING ABSOLUTE NODAL COORDINATE FORMULATION	**w56hzv-04-02-0001**
	5b. GRANT NUMBER
	5c. PROGRAM ELEMENT NUMBER
6. AUTHOR(S) **Hiroki Yamashita; Antti Valkeapaa; Paramsothy Jayakumar; Hiroyuki Sugiyama**	5d. PROJECT NUMBER
	5e. TASK NUMBER
	5f. WORK UNIT NUMBER
7. PERFORMING ORGANIZATION NAME(S) AND ADDRESS(ES) **Department of Mechanical and Industrial Engineering,The University of Iowa,2312 Seamans Center,Iowa City,IA,52242**	8. PERFORMING ORGANIZATION REPORT NUMBER **; #24515**
9. SPONSORING/MONITORING AGENCY NAME(S) AND ADDRESS(ES) **U.S. Army TARDEC, 6501 East Eleven Mile Rd, Warren, Mi, 48397-5000**	10. SPONSOR/MONITOR'S ACRONYM(S) **TARDEC**
	11. SPONSOR/MONITOR'S REPORT NUMBER(S) **#24515**

12. DISTRIBUTION/AVAILABILITY STATEMENT
Approved for public release; distribution unlimited

13. SUPPLEMENTARY NOTES
For ASME Journal of Computational Nonlinear Dynamics

14. ABSTRACT

In this investigation, a continuum mechanics based bi-linear shear deformable shell element is developed using the absolute nodal coordinate formulation for the large deformation analysis of multibody shell structures. The element consists of four nodes, each of which has the global position coordinates and the gradient coordinates along the thickness introduced for describing the orientation and deformation of the cross section of the shell element. The global position field on the mid-surface and the position vector gradient at a material point in the element are interpolated by bi-linear polynomials. The continuum mechanics approach is used to formulate the generalized elastic forces, allowing for the consideration of nonlinear constitutive models in a straightforward manner. The element locking exhibited in this type of element can be eliminated using the assumed natural strain (ANS) and enhanced assumed strain (EAS) approaches. In particular, the combined ANS and EAS approach is introduced to alleviate the thickness locking arising from the erroneous transverse normal strain distribution. Several numerical examples are presented in order to demonstrate the accuracy and the rate of convergence of numerical solutions obtained by the continuum mechanics based bi-linear shear deformable ANCF shell element proposed in this investigation.

15. SUBJECT TERMS

16. SECURITY CLASSIFICATION OF:			17. LIMITATION OF ABSTRACT	18. NUMBER OF PAGES	19a. NAME OF RESPONSIBLE PERSON
a. REPORT **unclassified**	b. ABSTRACT **unclassified**	c. THIS PAGE **unclassified**	**Public Release**	**42**	

Standard Form 298 (Rev. 8-98)
Prescribed by ANSI Std Z39-18

ABSTRACT

In this investigation, a continuum mechanics based bi-linear shear deformable shell element is developed using the absolute nodal coordinate formulation for the large deformation analysis of multibody shell structures. The element consists of four nodes, each of which has the global position coordinates and the gradient coordinates along the thickness introduced for describing the orientation and deformation of the cross section of the shell element. The global position field on the mid-surface and the position vector gradient at a material point in the element are interpolated by bi-linear polynomials. The continuum mechanics approach is used to formulate the generalized elastic forces, allowing for the consideration of nonlinear constitutive models in a straightforward manner. The element locking exhibited in this type of element can be eliminated using the assumed natural strain (ANS) and enhanced assumed strain (EAS) approaches. In particular, the combined ANS and EAS approach is introduced to alleviate the thickness locking arising from the erroneous transverse normal strain distribution. Several numerical examples are presented in order to demonstrate the accuracy and the rate of convergence of numerical solutions obtained by the continuum mechanics based bi-linear shear deformable ANCF shell element proposed in this investigation.

1. INTRODUCTION

The rectangular plate/shell elements of the absolute nodal coordinate formulation (ANCF) [1] can be classified into the fully parameterized shear deformable element [2,3] and the gradient deficient thin plate element [4,5]. While the fully parameterized element leads to a general motion description that accounts for complex coupled deformation modes of the plate/shell element, use of higher order polynomials and the coupled deformation modes exhibited in this type of element causes severe element locking and special care needs to be exercised to alleviate the locking [6]. The gradient deficient thin plate element, on the other hand, is developed by removing the position vector gradients along the thickness ($\partial \mathbf{r} / \partial z$), and the global displacement field on the mid-surface can be uniquely parameterized by the global position vector and the two gradient vectors $\partial \mathbf{r} / \partial x$ and $\partial \mathbf{r} / \partial y$ which are both tangent to the surface. By doing so, the cross section is assumed to be rigid and the elastic forces are derived using an in-plane stress assumption with Kirchhoff-Love plate theory. This leads to the non-conforming plate element in which the inter-element continuity is guaranteed, while the conforming thin plate element can be obtained by introducing the additional nodal coordinates $\partial^2 \mathbf{r} / \partial x \partial y$ with bi-cubic Hermite polynomials [4]. Despite the fact that the gradient deficient thin ANCF plate elements have proven to be successful in solving challenging engineering problems that involve large deformable thin plate and shell structures, consideration of general nonlinear constitutive models requires special formulations and implementation due to the in-plane stress assumption.

In recent years, an ANCF parameterization which does not include the position vector gradients tangent to the beam centerline and the mid-surface are investigated for shear deformable ANCF beam and plate elements. For beam problems, it is shown in the literature [7] that the elimination of the tangential slope vector along the beam centerline leads to accurate

elastic force descriptions due to weaker polynomial coupling between the displacement and gradient fields, and use of the general continuum mechanics approach for the elastic forces calculation allows for modeling curved beam structures in a straightforward manner. The assumed displacement field on the beam centerline does not involve slope coordinates, while the transverse slopes are employed to parameterize the orientation and deformation of the beam cross section. For plate elements, on the other hand, the position vector gradient along the thickness can be used to describe the orientation and deformation of the cross section of the plate element, and this parameterization leads to a shear deformable element that can capture the thickness deformation using the transverse slope vectors. That is, use of such an element parameterization leads to shear deformable plate elements while reducing the number of coordinates per node as discussed in the literature [8], in which a selective reduced integration is used to alleviate the transverse shear locking of the bi-linear shear deformable ANCF plate element. The element locking problem exhibited in the bi-linear shear deformable ANCF plate element is further investigated in the literature [9], in which the assumed natural strain (ANS) and the enhanced assumed strain (EAS) approaches are suggested to alleviate the transverse shear locking, thickness locking, and the in-plane normal/shear locking.

The elastic forces of the bi-linear shear deformable ANCF plate element in the literatures [8,9] are formulated based on the *elastic mid-plane approach*, in which the six strain components are evaluated on the *mid-plane* using Green-Lagrange strains and the approximated curvature expression is used to define the plate bending and twisting deformation. In other words, the strain distribution along the thickness is assumed to be constant in this approach, allowing for the evaluation of the elastic forces as an area element. Use of this element is limited to moderately thick flat plate problems due to the simplifying assumptions made in this model. Furthermore,

consideration of general nonlinear constitutive models requires special formulations and implementation as in the thin ANCF plate elements. Most challenging engineering problems that involves large deformable shell structures, on the other hand, call for accurate modeling of shell structures with various material nonlinearities, some of which include the modeling of rubber tires for vehicle/terrain interaction; wind turbine rotor blades made of composite materials; biomechanics applications with biomaterials; and many others. To achieve this goal, elastic forces of the shell element need to be developed as a continuum volume by considering the stress variation along the thickness using a general *continuum mechanics approach*, while the thickness locking can have an adverse impact on the accuracy as has been address for solid shell elements [10-13]. It is, therefore, the objective of this investigation to develop the continuum mechanics based bi-linear shear deformable shell element using the absolute nodal coordinate formulation.

The paper that discusses the development of the bi-linear shear deformable ANCF shell element using the continuum mechanics approach is organized as follows. In Section 2, the kinematics and parameterization of the bi-linear ANCF shell element are presented, while the elastic forces based on the general continuum mechanics approach and remedies for the element locking exhibited in the element are discussed in Section 3. In Section 4, the equations of motion and the solution procedure are discussed. Numerical results and comparison with existing plate/shell elements are presented in order to demonstrate the effect of the element locking on the accuracy for the continuum mechanics based bi-linear shear deformable ANCF shell element in Section 5. Summary and conclusions drawn from this study are presented in Section 6.

2. KINEMATICS OF BI-LINEAR SHEAR DEFORMABLE ANCF SHELL ELEMENT

As shown in Fig. 1, the global position vector $\mathbf{r}^i$ of a material point $\mathbf{x}^i = [x^i \quad y^i \quad z^i]^{\mathrm{T}}$ in shell element *i* is defined as

$$\mathbf{r}^i = \mathbf{r}_m^i(x^i, y^i) + z^i \frac{\partial \mathbf{r}_m^i}{\partial z^i}(x^i, y^i) \tag{1}$$

where $\mathbf{r}_m^i(x^i, y^i)$ is the global position vector on the mid-surface and $\partial \mathbf{r}_m^i(x^i, y^i)/\partial z^i$ is the transverse gradient vector used to describe the orientation and deformation of the infinitesimal volume in the element. The preceding global displacement field is interpolated using the bi-linear polynomials as follows:

$$r^i = a_0 + a_1 x^i + a_2 y^i + a_3 x^i y^i + z^i(a_4 + a_5 x^i + a_6 y^i + a_7 x^i y^i) \tag{2}$$

from which, one can interpolate both position vector on the mid-surface and the transverse gradient vector using the same bi-linear shape function matrix $\mathbf{S}_m^i$ as follows:

$$\mathbf{r}_m^i(x^i, y^i) = \mathbf{S}_m^i(x^i, y^i)\mathbf{e}_m^i, \qquad \frac{\partial \mathbf{r}_m^i}{\partial z^i}(x^i, y^i) = \mathbf{S}_m^i(x^i, y^i)\mathbf{e}_g^i \tag{3}$$

where $\mathbf{S}_m^i = \begin{bmatrix} S_1^i\mathbf{I} & S_2^i\mathbf{I} & S_3^i\mathbf{I} & S_4^i\mathbf{I} \end{bmatrix}$ and

$$S_1^i = \frac{1}{4}(1-\xi^i)(1-\eta^i),\ S_2^i = \frac{1}{4}(1+\xi^i)(1-\eta^i),\ S_3^i = \frac{1}{4}(1+\xi^i)(1+\eta^i),\ S_4^i = \frac{1}{4}(1-\xi^i)(1+\eta^i) \tag{4}$$

where $\xi^i = x^i/(\ell^i/2)$ and $\eta^i = y^i/(w^i/2)$. ℓ^i and w^i are lengths along the element x^i and y^i axes, respectively. In Eq. 3, the vectors $\mathbf{e}_m^i$ and $\mathbf{e}_g^i$ represent the element nodal coordinates associated with the global position vector on the mid-surface and the transverse gradient vector. That is, for node *k* of element *i*, one has $\mathbf{e}_m^{ik} = \mathbf{r}^{ik}$ and $\mathbf{e}_g^{ik} = \partial \mathbf{r}^{ik}/\partial z^i$. It is important to notice here that the assumed displacement field $\mathbf{r}_m^i$ defined on the mid-surface in Eq. 3 does not involve any gradient coordinates, while the orientation and deformation of the infinitesimal volume at the material point in the shell element is parameterized by the transverse gradient coordinates only. Substitution of Eq. 3 into Eq. 1 leads to the following general expression for the global position vector used for the absolute nodal coordinate formulation:

$$\mathbf{r}^i(x^i, y^i, z^i) = \mathbf{S}^i(x^i, y^i, z^i)\mathbf{e}^i \tag{5}$$

where the shape function matrix $\mathbf{S}^i$ and the element nodal coordinate vector $\mathbf{e}^i$ are, respectively, defined as

$$\mathbf{S}^i = \begin{bmatrix} \mathbf{S}^i_m & z^i\mathbf{S}^i_m \end{bmatrix}, \qquad \mathbf{e}^i = [(\mathbf{e}^i_m)^T \quad (\mathbf{e}^i_g)^T]^T \tag{6}$$

3. CONTINUUM MECHANICS BASED SHEAR DEFORMABLE ANCF SHELL ELEMENT

3.1 Generalized Elastic Forces using Continuum Mechanics Approach

In the continuum mechanics approach, the elastic forces of the shell element are evaluated as a continuum volume and the Green-Lagrange strain tensor **E** at an arbitrary material point in element *i* is defined as follows:

$$\mathbf{E}^i = \frac{1}{2}\left((\mathbf{F}^i)^T\mathbf{F}^i - \mathbf{I}\right) \tag{7}$$

where $\mathbf{F}^i$ is the displacement gradient tensor defined by

$$\mathbf{F}^i = \frac{\partial \mathbf{r}^i}{\partial \mathbf{X}^i} = \frac{\partial \mathbf{r}^i}{\partial \mathbf{x}^i}\left(\frac{\partial \mathbf{X}^i}{\partial \mathbf{x}^i}\right)^{-1} = \bar{\mathbf{J}}^i(\mathbf{J}^i)^{-1} \tag{8}$$

In the preceding equation, $\bar{\mathbf{J}}^i = \partial \mathbf{r}^i / \partial \mathbf{x}^i$ and $\mathbf{J}^i = \partial \mathbf{X}^i / \partial \mathbf{x}^i$, where the vector $\mathbf{X}^i$ represents the global position vector of element *i* at an arbitrary reference configuration. Substitution of Eq. 8 into Eq. 7 leads to

$$\mathbf{E}^i = (\mathbf{J}^i)^{-T}\tilde{\mathbf{E}}^i(\mathbf{J}^i)^{-1} \tag{9}$$

where $\tilde{\mathbf{E}}^i$ is the covariant strain tensor defined by

$$\tilde{\mathbf{E}}^i = \frac{1}{2}\left((\bar{\mathbf{J}}^i)^T\bar{\mathbf{J}}^i - (\mathbf{J}^i)^T\mathbf{J}^i\right) \tag{10}$$

The transformation (push-forward operation) of the covariant strain tensor $\tilde{\mathbf{E}}^i$ given by Eq. 9 can be re-expressed in a vector form by introducing the engineering covariant strain vector $\tilde{\boldsymbol{\varepsilon}}^i$ as

$$\boldsymbol{\varepsilon}^i = (\mathbf{T}^i)^{-T} \tilde{\boldsymbol{\varepsilon}}^i \tag{11}$$

where the vector $\boldsymbol{\varepsilon}$ in Eq. 11 is the engineering strain vector at the deformed configuration defined as

$$\boldsymbol{\varepsilon}^i = [\varepsilon^i_{xx} \quad \varepsilon^i_{yy} \quad \gamma^i_{xy} \quad \varepsilon^i_{zz} \quad \gamma^i_{xz} \quad \gamma^i_{yz}]^T \tag{12}$$

and the engineering covariant strain vector is defined as

$$\tilde{\boldsymbol{\varepsilon}}^i = [\tilde{\varepsilon}^i_{xx} \quad \tilde{\varepsilon}^i_{yy} \quad \tilde{\gamma}^i_{xy} \quad \tilde{\varepsilon}^i_{zz} \quad \tilde{\gamma}^i_{xz} \quad \tilde{\gamma}^i_{yz}]^T \tag{13}$$

The transformation matrix $\mathbf{T}^i$ in Eq. 11 can be expressed explicitly as

$$\mathbf{T}^i = \begin{bmatrix} (J^i_{11})^2 & (J^i_{12})^2 & 2J^i_{11}J^i_{12} & (J^i_{13})^2 & 2J^i_{11}J^i_{13} & 2J^i_{12}J^i_{13} \\ (J^i_{21})^2 & (J^i_{22})^2 & 2J^i_{21}J^i_{22} & (J^i_{23})^2 & 2J^i_{21}J^i_{23} & 2J^i_{22}J^i_{23} \\ J^i_{11}J^i_{21} & J^i_{12}J^i_{22} & J^i_{11}J^i_{22}+J^i_{12}J^i_{21} & J^i_{13}J^i_{23} & J^i_{11}J^i_{23}+J^i_{13}J^i_{21} & J^i_{12}J^i_{23}+J^i_{13}J^i_{22} \\ (J^i_{31})^2 & (J^i_{32})^2 & 2J^i_{31}J^i_{32} & (J^i_{33})^2 & 2J^i_{31}J^i_{33} & 2J^i_{32}J^i_{33} \\ J^i_{11}J^i_{31} & J^i_{12}J^i_{32} & J^i_{11}J^i_{32}+J^i_{12}J^i_{31} & J^i_{13}J^i_{33} & J^i_{11}J^i_{33}+J^i_{13}J^i_{31} & J^i_{12}J^i_{33}+J^i_{13}J^i_{32} \\ J^i_{21}J^i_{31} & J^i_{22}J^i_{32} & J^i_{21}J^i_{32}+J^i_{22}J^i_{31} & J^i_{23}J^i_{33} & J^i_{21}J^i_{33}+J^i_{23}J^i_{31} & J^i_{22}J^i_{33}+J^i_{23}J^i_{32} \end{bmatrix} \tag{14}$$

and J^i_{ab} is the element in the *a*-th column and *b*-th row of matrix $\mathbf{J}^i$ which is constant in time. The generalized elastic forces can then be obtained using the virtual work as follows:

$$\mathbf{Q}^i_k = \int_{V^i_0} \left(\frac{\partial \boldsymbol{\varepsilon}^i}{\partial \mathbf{e}^i} \right)^T \boldsymbol{\sigma}^i dV^i_0 \tag{15}$$

where $\boldsymbol{\sigma}^i$ is a vector of the second Piola–Kirchhoff stresses and dV^i_0 is the infinitesimal volume at the reference configuration of element *i*. It is important to notice here that the element elastic forces are evaluated as a continuum volume, and the stress vector for the shell element can be obtained with various nonlinear constitutive models for large deformation problems without ad hoc procedures.

3.2 Element Locking for Transverse Shear and In-Plane Shear/Normal Strains

As it has been addressed in literatures of shell element formulations [10-20], the bi-linear quadrilateral shell element suffer from the transverse shear locking and the in-plane shear/normal locking. The transverse shear locking can be eliminated using the assumed natural strain (ANS) approach proposed by Bathe and Dvorkin [16,17]. In this approach, the covariant shear strain components are interpolated using those evaluated at the sampling points *A, B, C* and *D* shown in Fig. 2 as follows:

$$\left.\begin{aligned} \tilde{\gamma}_{xz}^{ANS} &= \frac{1}{2}(1-\eta)\tilde{\gamma}_{xz}^{C} + \frac{1}{2}(1+\eta)\tilde{\gamma}_{xz}^{D} \\ \tilde{\gamma}_{yz}^{ANS} &= \frac{1}{2}(1-\xi)\tilde{\gamma}_{yz}^{A} + \frac{1}{2}(1+\xi)\tilde{\gamma}_{yz}^{B} \end{aligned}\right\} \tag{16}$$

where $\tilde{\gamma}_{xz}^{C}$, $\tilde{\gamma}_{xz}^{D}$, $\tilde{\gamma}_{yz}^{A}$ and $\tilde{\gamma}_{yz}^{B}$ are compatible covariant transverse shear strains at the sampling points.

The parasitic in-plane shear under pure bending loads is a typical locking problem exhibited in the bi-linear quadrilateral element [21], and the compatible in-plane strains (ε_{xx}, ε_{yy} and γ_{xy}) obtained by the assumed displacement field can be enhanced by introducing the enhanced assumed strains (EAS) $\boldsymbol{\varepsilon}^{EAS}$ as [14,15]

$$\boldsymbol{\varepsilon} = \boldsymbol{\varepsilon}^{c} + \boldsymbol{\varepsilon}^{EAS} \tag{17}$$

where $\boldsymbol{\varepsilon}^{c}$ indicates the compatible strain vector and the strain vector $\boldsymbol{\varepsilon}^{EAS}$ is defined by

$$\boldsymbol{\varepsilon}^{EAS}(\boldsymbol{\xi}) = \mathbf{G}(\boldsymbol{\xi})\boldsymbol{\alpha} \tag{18}$$

In the preceding equation, $\boldsymbol{\alpha}$ is a vector of internal parameters introduced to define the enhanced in-plane strain field and the matrix $\mathbf{G}(\boldsymbol{\xi})$ can be defined as [14,15]

$$\mathbf{G}(\boldsymbol{\xi}) = \frac{|\mathbf{J}_0|}{|\mathbf{J}(\boldsymbol{\xi})|}\mathbf{T}_0^{-\mathrm{T}}\mathbf{M}(\boldsymbol{\xi}) \tag{19}$$

where $\mathbf{J}(\boldsymbol{\xi})$ and $\mathbf{J}_0$ are displacement gradient matrices at the reference configuration evaluated at the Gaussian integration point $\boldsymbol{\xi}$ and at the center of element ($\boldsymbol{\xi} = \mathbf{0}$), respectively. $\boldsymbol{\xi}$ is a vector of the element coordinates in the parametric domain and $\mathbf{T}_0$ is the constant transformation matrix evaluated at the center of element as shown in Eq. 14. The matrix $\mathbf{M}(\boldsymbol{\xi})$ defines polynomials for the enhancement of the in-plane strain field in the parametric domain. For example, the linear distribution of in-plane strains (ε_{xx}, ε_{yy} and γ_{xy}) requires introducing the following interpolation matrix $\mathbf{M}(\boldsymbol{\xi})$:

$$\mathbf{M}(\boldsymbol{\xi}) = \begin{bmatrix} \xi & 0 & 0 & 0 \\ 0 & \eta & 0 & 0 \\ 0 & 0 & \xi & \eta \\ 0 & 0 & 0 & 0 \\ 0 & 0 & 0 & 0 \\ 0 & 0 & 0 & 0 \end{bmatrix} \tag{20}$$

where the additional four internal EAS parameters associated with the four columns of the matrix $\mathbf{M}(\boldsymbol{\xi})$ are introduced in this model. Using Eq. 19, the enhanced covariant strains are then pushed forward to those at the deformed configuration in the physical domain. It is important to notice here that the matrix $\mathbf{M}(\boldsymbol{\xi})$ needs to satisfy the following condition [14]:

$$\int \mathbf{M}(\boldsymbol{\xi}) d\boldsymbol{\xi} = \mathbf{0} \tag{21}$$

such that the orthogonality condition between the assumed stress and strain is satisfied as

$$\int_{V_0} \boldsymbol{\sigma} \cdot \boldsymbol{\varepsilon}^{EAS} dV_0 = 0 \tag{22}$$

Using the preceding condition, the unknown assumed stress term that appears in Hu-Washizu mixed variational principle vanishes and one can obtain the generalized elastic force vector as follows [14]:

$$\mathbf{Q}_k^i = -\int_{V_0^i} \left(\frac{\partial \boldsymbol{\varepsilon}^c}{\partial \mathbf{e}^i} \right)^T \frac{\partial W^i(\boldsymbol{\varepsilon}^c + \boldsymbol{\varepsilon}^{EAS})}{\partial \boldsymbol{\varepsilon}^i} dV_0^i \tag{23}$$

where W is an elastic energy function. For example, the elastic energy function W of the compressible neo-Hookean material model is defined as follows [22]:

$$W = \frac{\mu}{2}\left(\mathrm{tr}(\mathbf{C}) - 3\right) - \mu \ln J + \frac{\lambda}{2}\left(\ln J\right)^2 \tag{24}$$

where μ and λ are the Lamé constants; $\mathbf{C} = \mathbf{F}^T\mathbf{F}$ is the right Cauchy-Green deformation tensor; and $J = \det(\mathbf{F}) = \sqrt{\det(\mathbf{C})}$. It is important to notice here that the right Cauchy-Green deformation tensor that accounts for the enhanced assumed strain modification is defined as follows:

$$\mathbf{C} = 2(\mathbf{E}^c + \mathbf{E}^{EAS}) + \mathbf{I} \tag{25}$$

3.3 Thickness Locking

Use of the transverse gradients in the ANCF shell element introduces thickness deformation modes and the locking associated with the transverse normal strain is exhibited in the bi-linear shear deformable ANCF shell element. The solid shell elements which consists of layers of translational nodal coordinates at the top and bottom surfaces of the element [10-13] and shell elements parameterized by extensible directors [18-20] suffer from the similar thickness locking resulting from the erroneous transverse normal strain distribution. The use of the assumed natural strain (ANS) approach is proposed in the literature [18] to alleviate the thickness locking of the shell element modeled by extensible directors and the transverse normal strain at a material point in the element is approximated as follows:

$$\varepsilon_{zz}^{ANS} = S_1^{ANS}\varepsilon_{zz}^1 + S_2^{ANS}\varepsilon_{zz}^2 + S_3^{ANS}\varepsilon_{zz}^3 + S_4^{ANS}\varepsilon_{zz}^4 \tag{26}$$

where ε_{zz}^k indicates the compatible transverse normal strain at node *k* as shown in Fig. 2 and S_k^{ANS} is the shape function associated with it. This approach is applied to the bi-linear shear deformable ANCF flat plate element formulated with the elastic mid-plane approach [9] to alleviate the thickness locking problem. Since the strain distribution along the thickens is assumed to be constant and the stress is evaluated on the mid-surface, use of the assumed natural strain approach can alleviate the thickness locking effectively if the compatible transverse normal strains at four corners on the mid-surface are accurate enough. However, in the case of the continuum mechanics approach, the elastic forces are evaluated as a continuum volume and the transverse normal strain are evaluated at the integration points which do not lie on the mid-surface, thus better approximation of the transverse normal strain is needed to alleviate the thickness locking for the continuum mechanics based ANCF shell element.

It has been shown that the use of the enhanced assumed strain (EAS) approach leads to the better approximation of the transverse normal strain distribution and the thickness locking can be alleviated [11,19]. To this end, the additional internal EAS parameters associated with the enhanced transverse normal strain are added, and the interpolation matrix $\mathbf{M}(\boldsymbol{\xi})$ is augmented associated with it. For example, if the linear transverse normal strain term is introduced as a function of the thickness coordinate *z*, the interpolation matrix $\mathbf{M}(\boldsymbol{\xi})$ given in Eq. 19 is modified as

$$\mathbf{M}(\boldsymbol{\xi}) = \begin{bmatrix} \xi & 0 & 0 & 0 & 0 \\ 0 & \eta & 0 & 0 & 0 \\ 0 & 0 & \xi & \eta & 0 \\ 0 & 0 & 0 & 0 & \zeta \\ 0 & 0 & 0 & 0 & 0 \\ 0 & 0 & 0 & 0 & 0 \end{bmatrix} \tag{27}$$

where $\zeta = z/(h/2)$. It is important to notice here that there are no strain enhancement associated with the transverse shear strains γ_{xz} and γ_{yz} defined in the fifth and sixth rows. While there are zero sub-matrix associated with these strains in the matrix, the matrix $\mathbf{G}(\boldsymbol{\xi})$ define by Eq. 19 becomes a full matrix since the matrix $\mathbf{T}_0^{-\mathrm{T}}$ is defined as a 6×6 full matrix evaluated at an arbitrary reference configuration. In the literature [19], the transformation matrix $\mathbf{G}(\boldsymbol{\xi})$ associated with the enhanced in-plane and thickness strain terms are assumed to be decoupled and the approximated transformation matrix is used. In this investigation, the exact transformation matrix defined for the general three-dimensional stress state is considered.

To further improve the transverse normal strain distribution in the continuum mechanics based element, the compatible strain for the transverse normal strain is modified by the assumed natural strain approach defined by Eq. 26 as follows:

$$\varepsilon_{zz} = \varepsilon_{zz}^{ANS} + \varepsilon_{zz}^{EAS} \tag{28}$$

The similar approach is employed for solid shell elements in literature [11]. In this investigation, the combined ANS and EAS approach for the thickness locking is applied to the bi-linear shear deformable ANCF shell element. With this approach, the transverse normal strain improved by the ANS approach is further enhanced by the enhanced assumed strain approach. For application of the approach to the continuum mechanics based ANCF shell element, the covariant strain components of the transverse shear and transverse normal strains are interpolated in the natural

coordinate domain first and then the covariant strain vector given in Eq. 13 is replaced with the following strain vector:

$$\tilde{\boldsymbol{\varepsilon}} = \begin{bmatrix} \tilde{\varepsilon}_{xx} & \tilde{\varepsilon}_{yy} & \tilde{\gamma}_{xy} & \tilde{\varepsilon}_{zz}^{ANS} & \tilde{\gamma}_{xz}^{ANS} & \tilde{\gamma}_{yz}^{ANS} \end{bmatrix}^T \tag{29}$$

The Green-Lagrange strains associated with the preceding covariant strains are evaluated using the transformation defined by Eq. 11. Having obtained the modified compatible strains, the enhanced assumed strains defined by Eq. 18 that considers the strain enhancement of the in-plane shear/normal as well as the transverse normal strains are added to them with the interpolation matrix $\mathbf{M}(\boldsymbol{\xi})$ given by Eq. 27. This leads to a systematic derivation of the generalized elastic forces of the locking-free continuum mechanics based shear deformable ANCF shell element.

4. EQUATIONS OF MOTION AND SOLUTION PROCEDURES

Using the principle of virtual work in dynamics, the equations of motion of the shear deformable ANCF shell element *i* can be expressed as

$$\mathbf{M}^i \ddot{\mathbf{e}}^i = \mathbf{Q}_k^i(\mathbf{e}^i, \boldsymbol{\alpha}^i) + \mathbf{Q}_e^i(\mathbf{e}^i, \dot{\mathbf{e}}^i, t) \tag{30}$$

where the vectors $\mathbf{Q}_k^i$ and $\mathbf{Q}_e^i$ are, respectively, the element elastic and external force vectors; and the matrix $\mathbf{M}^i$ is the constant element mass matrix defined by

$$\mathbf{M}^i = \int_{V_0^i} \rho_0^i (\mathbf{S}^i)^T \mathbf{S}^i dV_0^i \tag{31}$$

where ρ_0^i is the material density at the reference configuration. It is important to notice here that the generalized elastic forces are defined as a function of the nodal coordinates and the internal EAS parameters $\boldsymbol{\alpha}^i$. The parameter $\boldsymbol{\alpha}^i$ are determined by solving the following equation for each element:

$$\mathbf{h}^i(\mathbf{e}^i,\boldsymbol{\alpha}^i)=\int_{V_0^i}\left(\frac{\partial\boldsymbol{\varepsilon}^{EAS}}{\partial\boldsymbol{\alpha}^i}\right)^T\frac{\partial W^i(\boldsymbol{\varepsilon}^c+\boldsymbol{\varepsilon}^{EAS})}{\partial\boldsymbol{\varepsilon}^i}dV_0^i=\mathbf{0},\qquad i=1,\cdots,ne \tag{32}$$

The nodal coordinates $\mathbf{e}^i$ and the EAS internal parameters $\boldsymbol{\alpha}^i$ are determined at every time step such that both Eqs. 30 and 32 are satisfied. Using the time integration scheme in Newmark-β family, the nodal acceleration and velocity vectors at time step t_{n+1} are discretized in time as

$$\left.\begin{aligned}\ddot{\mathbf{e}}_{n+1}&=\frac{1}{\beta h^2}(\mathbf{e}_{n+1}-\mathbf{e}_n)-\frac{1}{\beta h}\ \dot{\mathbf{e}}_n-(\frac{1}{2\beta}-1)\ddot{\mathbf{e}}_n\\ \dot{\mathbf{e}}_{n+1}&=\frac{\gamma}{\beta h}(\mathbf{e}_{n+1}-\mathbf{e}_n)-(\frac{\gamma}{\beta}-1)\ \dot{\mathbf{e}}_n-h(\frac{\gamma}{2\beta}-1)\ddot{\mathbf{e}}_n\end{aligned}\right\} \tag{33}$$

Using the preceding equations, the equations of motion given by Eq. 30 can be expressed as a function of unknown variables $\mathbf{e}^i_{n+1}$ and $\boldsymbol{\alpha}^i_{n+1}$ as follows:

$$\mathbf{f}^i(\mathbf{e}^i_{n+1},\boldsymbol{\alpha}^i_{n+1})=\mathbf{0} \tag{34}$$

In other words, one needs to seek solutions to the following equations at time step t_{n+1}:

$$\mathbf{g}^i(\mathbf{e}^i_{n+1},\boldsymbol{\alpha}^i_{n+1})=\begin{bmatrix}\mathbf{f}^i(\mathbf{e}^i_{n+1},\boldsymbol{\alpha}^i_{n+1})\\ \mathbf{h}^i(\mathbf{e}^i_{n+1},\boldsymbol{\alpha}^i_{n+1})\end{bmatrix}=\mathbf{0} \tag{35}$$

Using Newton-Raphson method, Newton difference for $\mathbf{e}^i_{n+1}$ and $\boldsymbol{\alpha}^i_{n+1}$ can be obtained by solving the following matrix equation:

$$\begin{bmatrix}\partial\mathbf{f}^i/\partial\mathbf{e}^i_{n+1} & \partial\mathbf{f}^i/\partial\boldsymbol{\alpha}^i_{n+1}\\ \partial\mathbf{h}^i/\partial\mathbf{e}^i_{n+1} & \partial\mathbf{h}^i/\partial\boldsymbol{\alpha}^i_{n+1}\end{bmatrix}\begin{bmatrix}\Delta\mathbf{e}^i_{n+1}\\ \Delta\boldsymbol{\alpha}^i_{n+1}\end{bmatrix}=\begin{bmatrix}\mathbf{f}^i\\ \mathbf{h}^i\end{bmatrix} \tag{36}$$

Using the preceding equation, $\Delta\mathbf{e}^i_{n+1}$ can be obtained as a solution to the following equation:

$$\left(\frac{\partial\mathbf{f}^i_{n+1}}{\partial\mathbf{e}^i_{n+1}}-\frac{\partial\mathbf{f}^i_{n+1}}{\partial\boldsymbol{\alpha}^i_{n+1}}\left(\frac{\partial\mathbf{h}^i_{n+1}}{\partial\boldsymbol{\alpha}^i_{n+1}}\right)^{-1}\frac{\partial\mathbf{h}^i_{n+1}}{\partial\mathbf{e}^i_{n+1}}\right)\Delta\mathbf{e}^i_{n+1}=\mathbf{f}^i_{n+1}-\frac{\partial\mathbf{f}^i_{n+1}}{\partial\boldsymbol{\alpha}^i_{n+1}}\left(\frac{\partial\mathbf{h}^i_{n+1}}{\partial\boldsymbol{\alpha}^i_{n+1}}\right)^{-1}\mathbf{h}^i_{n+1} \tag{37}$$

The preceding equation is iteratively solved until $\mathbf{g}^i(\mathbf{e}^i_{n+1},\boldsymbol{\alpha}^i_{n+1})=\mathbf{0}$ defined by Eq. 35 is satisfied.

The internal EAS parameters are determined in each iteration step using the following update scheme:

$$\boldsymbol{\alpha}_{k+1}^{i} = \boldsymbol{\alpha}_{k}^{i} - (\mathbf{H}^{i})^{-1}\mathbf{h}^{i}(\mathbf{e}^{i}, \boldsymbol{\alpha}_{k}^{i}) \tag{38}$$

where Jacobian matrix $\mathbf{H}^{i}$ in the preceding equation is defined by:

$$\mathbf{H}^{i} = \frac{\partial \mathbf{h}^{i}}{\partial \boldsymbol{\alpha}^{i}} = \int_{V_0^i} (\mathbf{G}^{i})^{T} \frac{\partial^2 W^{i}(\boldsymbol{\varepsilon}^{c} + \boldsymbol{\varepsilon}^{EAS})}{\partial \boldsymbol{\varepsilon}^{i\,2}} \mathbf{G}^{i}\, dV_0^{i} \tag{39}$$

where the matrix $\mathbf{G}^{i}$ is defined by Eq. 19. The term $\partial^2 W / \partial \boldsymbol{\varepsilon}^2$ leads to a material moduli matrix obtained by the second derivative of the elastic energy function. That is, for a linear elasticity material model, this matrix is constant. However, for general nonlinear material models, the material moduli matrix is no longer constant and the iterative solution procedure is required to determine the internal EAS parameters $\boldsymbol{\alpha}^{i}$ for each element.

5. NUMERICAL RESULTS

In this section, several numerical examples are presented in order to demonstrate the performance of the continuum mechanics based bi-linear shear deformable ANCF shell element developed in this investigation. The effect of the assumed natural strain (ANS) and enhanced assumed strain (EAS) approaches on the element accuracy is also discussed.

5.1 Cantilevered Plate and Shell Subjected to a Point Force

In the first problem, a rectangular cantilevered plate subjected to a vertical point force at one of the corners of the plate is considered as shown in Fig. 3. The length, width and thickness of the plate are assumed to be 1.0 m, 1.0 m and 0.01 m. The Young's modulus and Poisson's ratio are assumed to be 2.1×10^{8} Pa and 0.3, respectively. As shown in Fig. 3, the plate is subjected to large deformation at the static equilibrium state. The six models with different strain

modifications discussed in Section 3 are considered to demonstrate the effect of the EAS and ANS approaches on the element convergence and accuracy. These models are summarized in Table 1. In Model-1, no strain modifications are made, while Model-2 is used to demonstrate the effect of the ANS approach to alleviate the transverse shear locking for the ANCF shell element. A comparison between Model-3 and 4 demonstrates the effect of the in-plane shear/normal locking alleviated by the EAS approach, while a comparison between Model-4, 5 and 6 demonstrates the use of the three different approaches for elimination of the thickness locking, i.e., the ANS (Model-4), the EAS (Model-5), and the combined ANS and EAS (Model-6) approaches as discussed in Section 3.3.

To measure the accuracy, error in solution is defined by a deviation of the vertical deflection at the force application point on the plate from that of the reference solution obtained by ANSYS SHELL181 with 100×100 elements. The numerical convergence of the solution is presented in Fig. 4 for each model. The numerical result obtained by the bi-linear shear deformable ANCF flat plate element based on the elastic mid-plane approach [9] is also presented in this figure for comparison. It is observed from the comparison between Model-1 and Model-2 that the accuracy is improved by alleviating the transverse shear locking with the ANS approach. However, the solution is converged to the erroneous solution. While the use of the EAS for the in-plane shear/normal locking and the ANS for the thickness locking slightly improve the rate of convergence, the convergent solution is still incorrect. It is important to notice that use of Model-6 with the combined ANS and EAS approach leads to the same result with that of the locking-free ANCF plate element based on the elastic mid-plane approach. This plate element employs ANS for alleviating the thickness locking. In other words, the strain modification used in the elastic mid-plane ANCF shell element corresponds to Model-4 in Table

1. However, Model-4 of the continuum mechanics based ANCF shell element leads to an erroneous solution due to the thickness locking. While the application of the EAS approach to the thickness locking improves the element performance as shown in the result of Model-5, the accuracy is not at satisfactory level especially when the small number of elements is used. This result clearly indicates severity of the thickness locking exhibited in the continuum mechanics based shear deformable ANCF shell element and the locking for the continuum mechanics based ANCF shell element needs to be eliminated using the combined EAS and ANS approach as demonstrated by the result of Model-6.

In the second problem, the flat plate is replaced with the quarter cylinder modeled by the continuum mechanics based bi-linear ANCF shell elements as shown in Fig. 5, and the radius of curvature is assumed to be 1.0 m. The material properties, tip load, width and height are the same as the previous example. The deformed shape at the static equilibrium state is shown in Fig. 5 and the large deformation is exhibited in this problem. As in the previous example, error in solution is defined by a deviation of the vertical deflection at the force application point from that of the reference solution obtained by ANSYS SHELL181 with 100×100 elements. The numerical convergence in solution is presented in Fig. 6 for Models 1 to 6 and ANSYS SHELL181 for comparison. The overall trend of the numerical convergence of solutions obtained by different models is similar to that observed for the flat plate problem. The result clearly indicate that use of the combine EAS and ANS approach leads to the ideal rate of convergence and accuracy for the shell structure.

5.2 Pinched Semi-Cylindrical Shell

A semi-cylindrical shell as shown in Fig. 7 subjected to a pinching force of 800 N at the middle of the free-hanging circumferential periphery is discussed. This problem is used as a benchmark

problem for various shell elements [13,23,24,25] and the numerical solution obtained by the proposed continuum mechanics based bi-linear shear deformable shell element (Model-6) is compared with those in the literatures [13,24,25]. The length, radius and thickness are assumed to be 3.048 m, 1.016 m and 0.03 m, respectively. Young's modulus and Poisson's ratio are assumed to be 2.0685×10^7 Pa and 0.3, respectively [13,23,24,25]. A quarter cylinder model with the symmetric boundary condition is used in the analysis. The deformed shape of the semi-cylindrical shell is shown in Fig. 7, and the nonlinear load-deflection curve shown in Fig. 8 agree well with those presented in the literatures [13,24,25]. Use of the 16×16 elements leads to the convergent solution in the case of the continuum mechanics based bi-linear shear deformable ANCF shell element.

5.3 Slit Annular Plate Subjected to Lifting Force

In the next example, a slit annular plate subjected to a lifting line force is considered as shown in Fig. 9. This problem is also widely used as a benchmark problem for shell elements [23]. The inside and outside radii of the annular plate are assumed to be 6.0 m and 10.0 m, respectively. Young's modulus and Poisson's ratio are assumed to be 2.1×10^7 Pa and $\nu=0.0$, respectively [23]. One end of the slit is fully clamped, while the other end of the slit is subjected to the line force of 50 N. The load-deflection curves at Point A and B shown in Fig. 10 are compared with those obtained using ANSYS SHELL181 with 10×60 elements as a reference solution and the results are in good agreement with those obtained by the continuum mechanics based bi-linear shear deformable ANCF shell element.

5.4 Natural Frequencies of Square Plate

The eignefrequency analysis of a square plate with free boundaries studied in the literatures

[6,26] is performed in this example. The dimensionless natural frequencies defined by $\boldsymbol{\Omega} = \boldsymbol{\omega} / \boldsymbol{\omega}_0$ with $\boldsymbol{\omega}_0 = \pi^2 \sqrt{D / \rho h l^4}$ are used, where D, ρ, h and l are $D = Eh^3 / 12(1-\nu^2)$, the material density, height and length of the plate, respectively. The first ten dimensionless eigenfrequencies are summarized in Table 2 for Model-6 that employs the combined ANS and EAS approach for the thickness locking. Use of the proposed low-order continuum mechanics based shear deformable shell element leads to better rate of convergence than the higher-order fully parameterized ANCF element presented in literatures [6,26].

5.5 Quarter Cylinder Pendulum

In the last problem, the nonlinear dynamic analysis of a shell structure with a nonlinear material model is considered. A quarter cylinder that has the same dimension as the one in Section 5.1 is used, and a compressible neo-Hookean material model is used to demonstrate the use of the nonlinear material model in the continuum mechanics based ANCF shell element developed in this investigation. The Lamé constants μ and λ are assumed to be 8.077×10^7 Pa and 1.212×10^7 Pa, respectively. The corner of the quarter cylinder is connected to the ground by a spherical joint. The deformed shapes of the quarter cylinder under the effect of gravity are shown in Fig. 11, in which the shell experiences large deformation. The global X, Y and Z position at point A shown in Fig. 11 are presented in Figs. 12-14 for different number of elements, and it is shown that use of 32×32 elements leads to the convergent solution.

6. SUMMARY AND CONCLUSIONS

In this investigation, a continuum mechanics based bi-linear shear deformable shell element is developed using the absolute nodal coordinate formulation for the large deformation analysis of multibody shell structures. The elastic forces are formulated using the continuum mechanics

approach which allows for the consideration of nonlinear material models such as hyperelasticity in the shell element in a straight forward manner. By doing so, the stress distribution along the thickness is considered and the elastic forces are evaluated as a continuum volume. It is demonstrated by some numerical examples that use of the combined EAS and ANS approach alleviates the thickness locking effectively exhibited in the continuum mechanics based bi-linear shear deformable ANCF shell element, while the transverse shear locking as well as the in-plane shear/normal strain locking can be alleviated by the ANS and EAS, respectively. The locking-free shear deformable element developed in this investigation can be used for modeling large deformable multibody shell structures in challenging engineering problems with material nonlinearities that include the modeling of rubber tires for vehicle/terrain interaction, wind turbine rotor blades made of composite materials, and biomechanics applications with biomaterials.

ACKNOWLEDGEMENTS

The authors wish to acknowledge the financial support of the Automotive Research Center (ARC) in accordance with Cooperative Agreement W56HZV-04-2-0001 U.S. Army Tank Automotive Research, Development and Engineering Center (TARDEC). Financial support for the last author received from FunctionBay Inc is acknowledged.

REFERENCES

[1] Gerstmayr, J., Sugiyama, H. and Mikkola, A., 2013, "Review on the Absolute Nodal Coordinate Formulation for Large Deformation Analysis of Multibody Systems", *ASME Journal of Computational and Nonlinear Dynamics*, vol. 8, pp. 031016-1-12.

[2] Mikkola, A. M., and Shabana, A. A., 2003, "A Non-Incremental Finite Element Procedure for The Analysis of Large Deformation of Plates and Shells in Mechanical System Applications", *Multibody System Dynamics*, vol. 9, pp.283-309.

[3] Mikkola, A.M.; Matikainen, M.K., 2006, "Development of Elastic Forces for a Large Deformation Plate Element Based on the Absolute Nodal Coordinate Formulation". *ASME Journal of Computational and Nonlinear Dynamics*, vol. 1, pp. 103-108, 2006.

[4] Dmitrochenko, O. and Pogorelov, D. Y., 2003, "Generalization of Plate Finite Elements for Absolute Nodal Coordinate Formulation", *Multibody System Dynamics*, vol. 10, pp. 17-43.

[5] Dufva, K., and Shabana, A. A., 2005, "Analysis of Thin Plate Structures Using The Absolute Nodal Coordinate Formulation", *IMechE Journal of Multi-body Dynamics*, vol. 219, pp. 345-355.

[6] Schwab, A. L., Gerstmayr, J., and Meijaard, J. P., 2007, "Comparison of Three-Dimensional Flexible Thin Plate Elements for Multibody Dynamic Analysis: Finite Element Formulation and Absolute Nodal Coordinate Formulation", *Proceedings of the ASME 2007 International Design Engineering Technical Conferences & Computers and Information in Engineering Conference*, Las Vegas, Nevada, USA.

[7] Nachbagauer, K., Gruber, P., and Gerestmayr, J., 2013, "Structural and Continuum Mechanics Approaches for a 3D shear Deformable ANCF Beam Finite Element:

Application to Static and Linearized Dynamic Examples", *ASME Journal of Computational and Nonlinear Dynamics*, vol. 8, pp.021004-1-7

[8] Dmitrochenko, O., Matikainen, M., and Mikkola, A., 2012, "The Simplest 3- and 4-Noded Fully Parameterized ANCF Plate Elements", *Proceedings of the ASME 2012 International Design Engineering Technical Conferences & Computers and Information in Engineering Conference*, Chicago, IL, USA

[9] Valkeapää, A. I., Yamashita, H., Jayakumar, P. and Sugiyama, H., "Gradient Deficient Bi-Linear Plate Element Based on Absolute Nodal Coordinate Formulation", in preparation.

[10] Sze, K. Y., 2002, "Three-Dimensional Continuum Finite Element Models for Plate/Shell Analysis", *Progress in Structural Engineering and Materials*, vol. 4, pp.400-407.

[11] Vu-Quoc, L., and Tan, X. G., 2003, "Optimal Solid Shells for Non-Linear Analyses of Multilayer Composites: I Statics", *Computer Methods in Applied Mechanics and Engineering*, vol. 192, pp. 975-1016.

[12] Vu-Quoc, L., and Tan, X. G., 2003, "Optimal Solid Shells for Non-Linear Analyses of Multilayer Composites: II Dynamics", *Computer Methods in Applied Mechanics and Engineering*, vol. 192, pp. 1017-1059.

[13] Mostafa, M., Sivaselvan, M. V. and Felippa, C. A., 2013, "A Solid-Shell Corotational Element Based on ANDES, ANS and EAS for Geometrically Nonlinear Structural Analysis", *International Journal for Numerical Methods in Engineering*, vol. 95, pp.145-180.

[14] Simo, J. C., and Rifai, M. S., 1990, "A Class of Mixed Assumed Strain Methods and The Method of Incompatible Modes", *International Journal for Numerical Methods in Engineering*, vol. 29, pp.1595-1638.

[15] Andelfinger, U., and Ramm, E., 1993, "EAS-Elements for Two-Dimensional, Three-Dimensional, Plate and Shell Structures and Their Equivalence to HR-Elements", *International Journal for Numerical Methods in Engineering*, vol. 36, pp.1311-1337.

[16] Dvorkin, E. N., and Bathe, K. J., 1984, "A Continuum Mechanics Based Four-Node Shell Element for General Non-Linear Analysis", *Engineering Computations*, vol. 1, pp.77-88.

[17] Bathe, K. J. and Dvorkin, E. N., 1986, "A Formulation of General Shell Elements - The Use of Mixed Interpolation of Tensorial Components", *International Journal for Numerical Methods in Engineering*, vol. 22, pp.697-722.

[18] Betsch, P., and Stein, E., 1995, "An Assumed Strain Approach Avoiding Artificial Thickness Straining for A Non-Linear 4-Node Shell Element", *Communications in Numerical Methods in Engineering*, vol. 11, pp. 899-909.

[19] Betsch, P., Gruttmann, F., and Stein, E., 1996, "A 4-Node Finite Shell Element for the Implementation of General Hyperelastic 3D-Elasticity at Finite Strains", *Computer Methods in Applied Mechanics and Engineering*, vol. 130, pp. 57-79.

[20] Bischoff, M., Ramm, E., 1997, "Shear Deformable Shell Elements for Large Strains and Rotations", *International Journal for Numerical Methods in Engineering*, vol. 40, pp.4427-4449.

[21] Cook, R. D., Malkus, D. S., Plesha, M. E., and Witt, R. J., 2002, *Concepts and Applications of Finite Element Analysis Fourth Edition*, Wiley.

[22] Bonet, J., and Wood, D. R., 1997, *Nonlinear Continuum Mechanics For Finite Element Analysis*, Cambridge University Press.

[23] Sze, K. Y., Liu, H. X., Lo, S. H., 2004, "Popular Benchmark Problems for Geometric Nonlinear Analysis of Shells", *Finite Elements in Analysis and Design*, vol. 40, pp.1551-1569.

[24] Stander, N., Matzenmiller, A., Ramm, E, 1988, "An Assessment of Assumed Strain Methods in Finite Rotation Shell Analysis", *Engineering Computations*, vol. 6, pp.58-66.

[25] Parisch, H., 1991, "An Investigation of a Finite Rotation Four Node Assumed Strain Shell Element", *International Journal for Numerical Methods in Engineering*, vol. 31, pp.127-15022.

[26] Matikainen, M.K., Valkeapää, A. I., Mikkola, A. M., and Schwab, A. L., 2013, "A Study of Moderately Thick Quadrilateral Plate Elements Based on the Absolute Nodal Coordinate Formulation", *Multibody System Dynamics*, pp. 1–30.

TABLE CAPTIONS

Table 1. Models for continuum mechanics assumption

Table 2. First ten dimensionless eigenfrequencies $\boldsymbol{\Omega} = \boldsymbol{\omega} / \boldsymbol{\omega}_0$ of the free (FFFF) square plate

FIGURE CAPTIONS

Figure 1. Kinematics of bi-linear ANCF element

Figure 2. Sampling points for assumed natural strain

Figure 3. Deformed shape of a cantilevered plate subjected to a large transverse tip load

Figure 4. Numerical convergence with large deformation (initially flat)

Figure 5. Deformed shape of a cantilevered plate subjected to a large transverse tip load

Figure 6. Numerical convergence with large deformation (initially curved)

Figure 7. Deformed shape of pinched semi-cylindrical shell

Figure 8. Load-deflection curve of pinched semi-cylindrical shell

Figure 9. Deformed shape of slit annular plate subjected to lifting force

Figure 10. Load-deflection curve of slit annular plate subjected to lifting force

Figure 11. Deformed shapes of quarter-cylindrical shell pendulum

Figure 12. Global X-position at Point A

Figure 13. Global Y-position at Point A

Figure 14. Global Z-position at Point A

Table 1. Strain modification for the continuum mechanics based ANCF bi-linear shell element

Model name	ANS for transverse shear strains ($\varepsilon_{xz}^{\text{ANS}}, \varepsilon_{yz}^{\text{ANS}}$)	EAS for in-plane strains ($\varepsilon_{xx}^{\text{EAS}}, \varepsilon_{yy}^{\text{EAS}}, \gamma_{xy}^{\text{EAS}}$)	ANS for transverse normal strain ($\varepsilon_{zz}^{\text{ANS}}$)	EAS for transverse normal strain ($\varepsilon_{zz}^{\text{EAS}}$)	Combined EAS and EAS for transverse normal strain ($\varepsilon_{zz}^{\text{ANS/EAS}}$)
Model-1	-	-	-	-	-
Model-2	Y	-	-	-	-
Model-3	Y	-	Y	-	-
Model-4	Y	Y	Y	-	-
Model-5	Y	Y	-	Y	-
Model-6	Y	Y	-	-	Y

Table 2. First ten dimensionless eigenfrequencies $\boldsymbol{\Omega} = \boldsymbol{\omega} / \boldsymbol{\omega}_0$ of the free (FFFF) square plate

1x1	2x2	4x4	8x8	16x16	Analytical solution
1.4328	1.4383	1.4014	1.3734	1.3548	1.3646
101.5117	2.3477	2.1142	2.0141	1.9721	1.9855
101.7252	3.1993	2.7186	2.5169	2.4415	2.4591
101.7288	4.0870	3.8097	3.6023	3.5267	3.5261
115.9849	4.0906	3.8172	3.6153	3.5524	3.5261
115.9849	7.5903	7.4061	6.7273	6.2849	6.1900
138.3927	98.8943	8.4204	6.7365	6.2862	6.1900
138.6304	98.8949	8.4332	6.7394	6.5196	6.4528
152.2271	101.7244	8.7211	7.4840	7.1160	7.0181
152.4032	101.7288	10.5372	8.5216	7.9556	7.8191

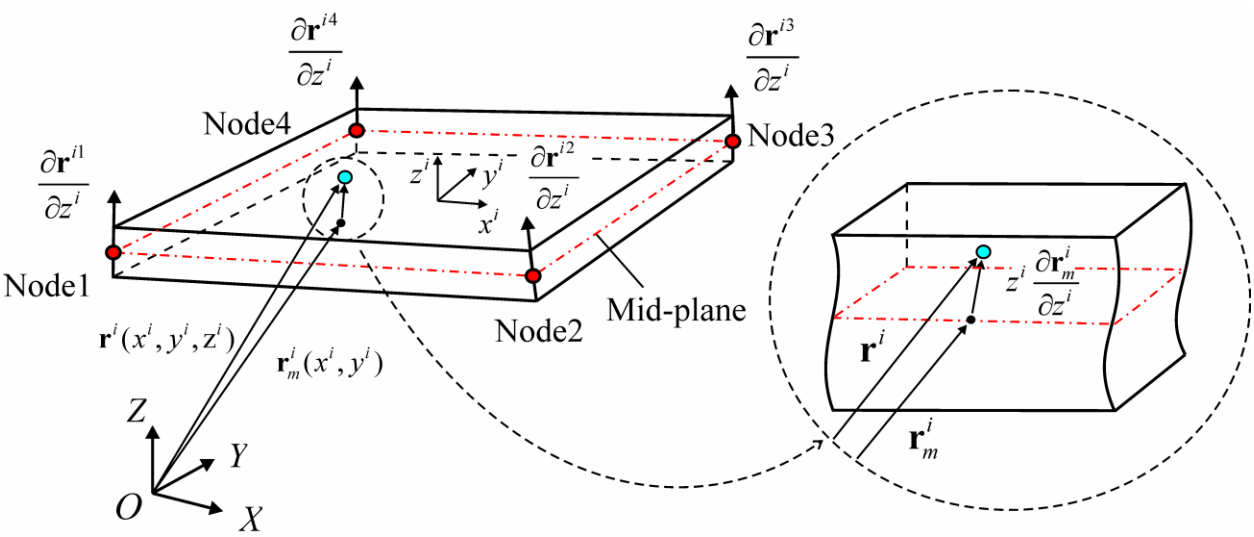

Figure 1. Kinematics of bi-linear shear deformable ANCF shell element

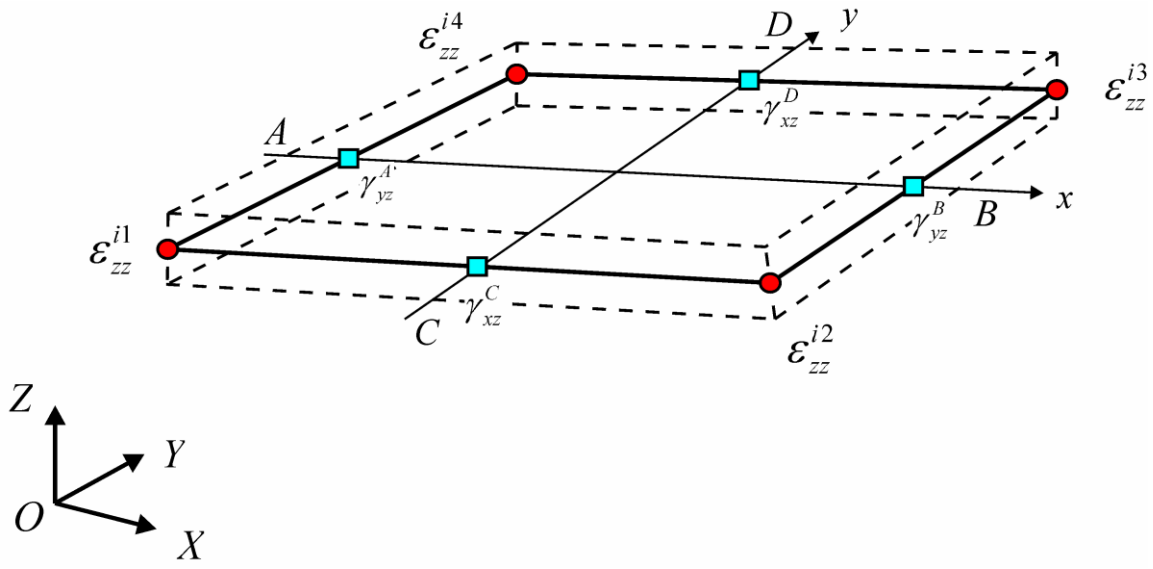

Figure 2. Sampling points for assumed natural strain

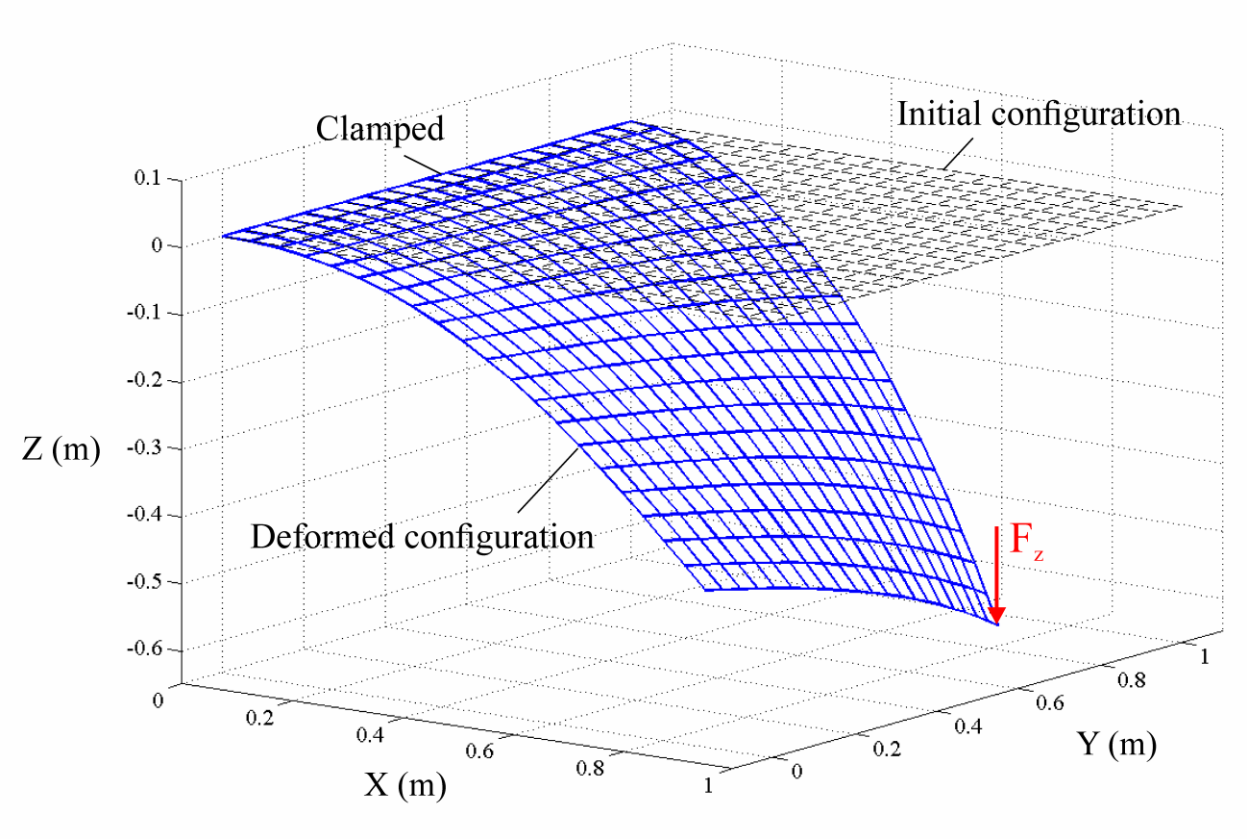

Figure 3. Deformed shape of a cantilevered plate subjected to a tip force

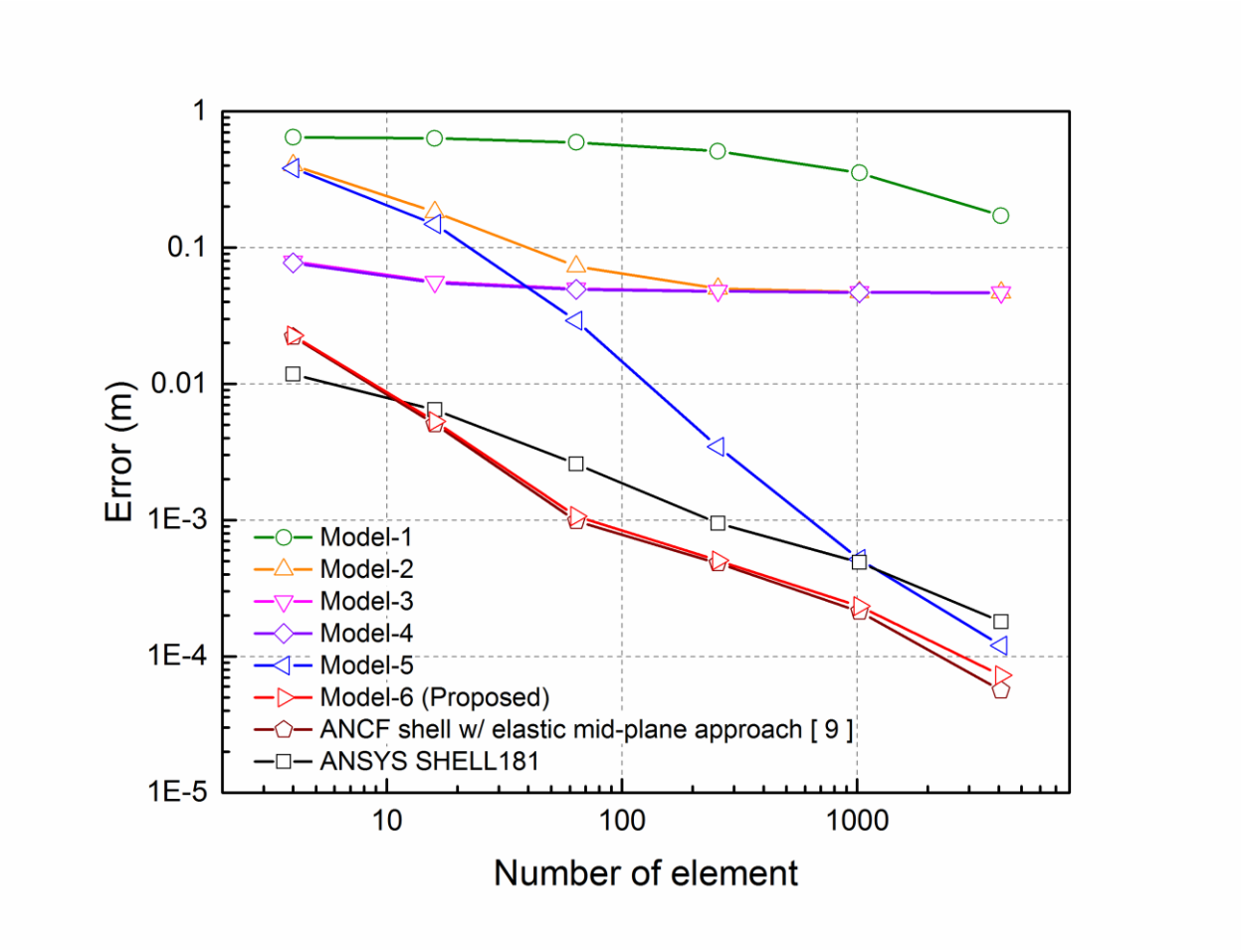

Figure 4. Numerical convergence of ANCF shell solutions: cantilevered plate subjected to a tip force with large deformation

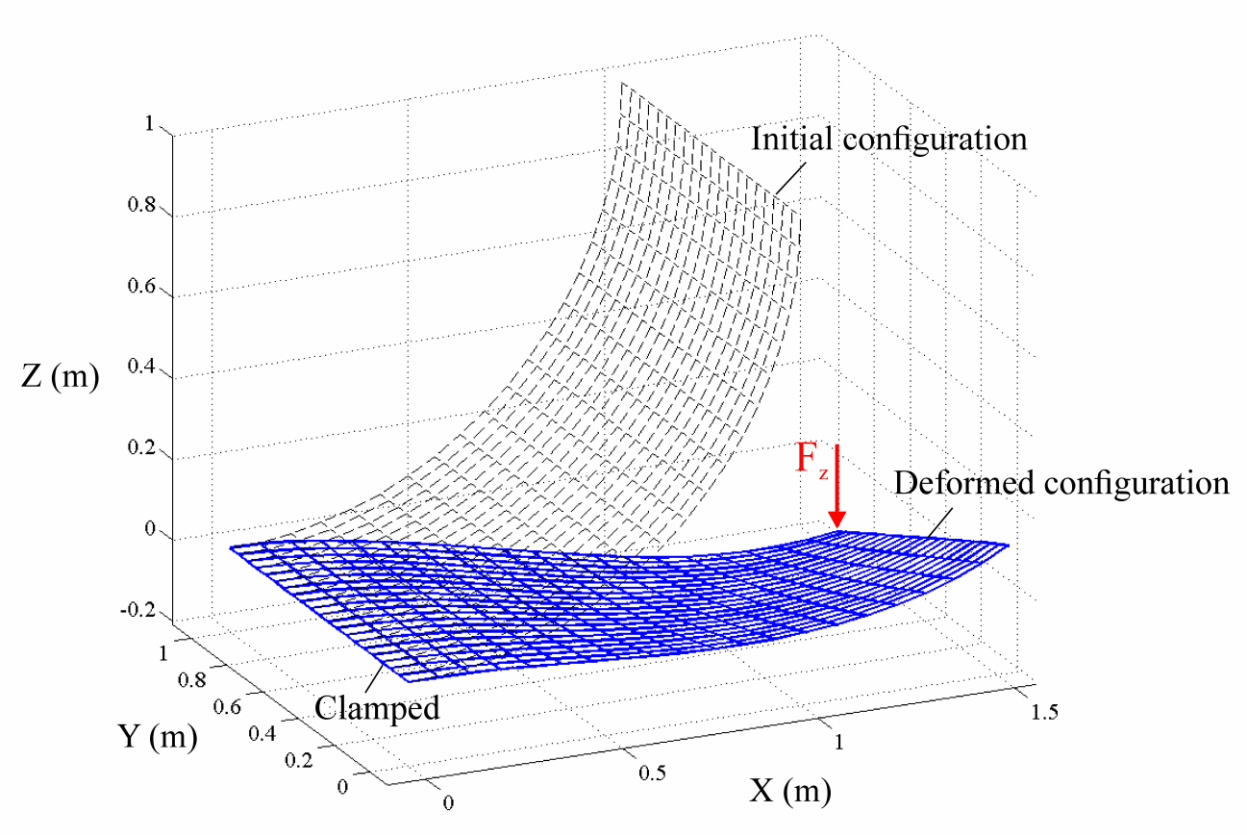

Figure 5. Deformed shape of a quarter cylinder subjected to a tip force

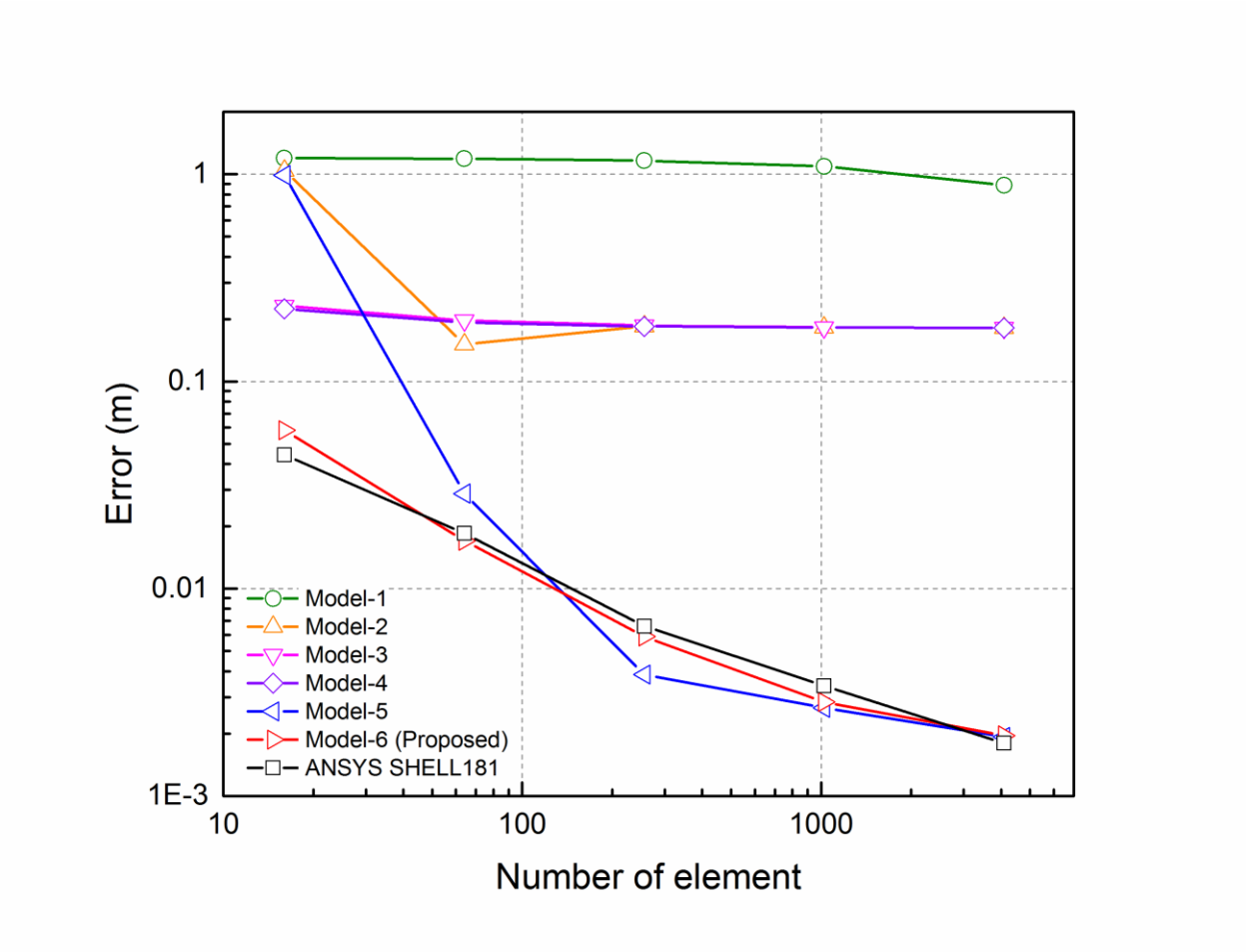

Figure 6. Numerical convergence of ANCF shell solutions: quarter cylinder subjected to a tip force

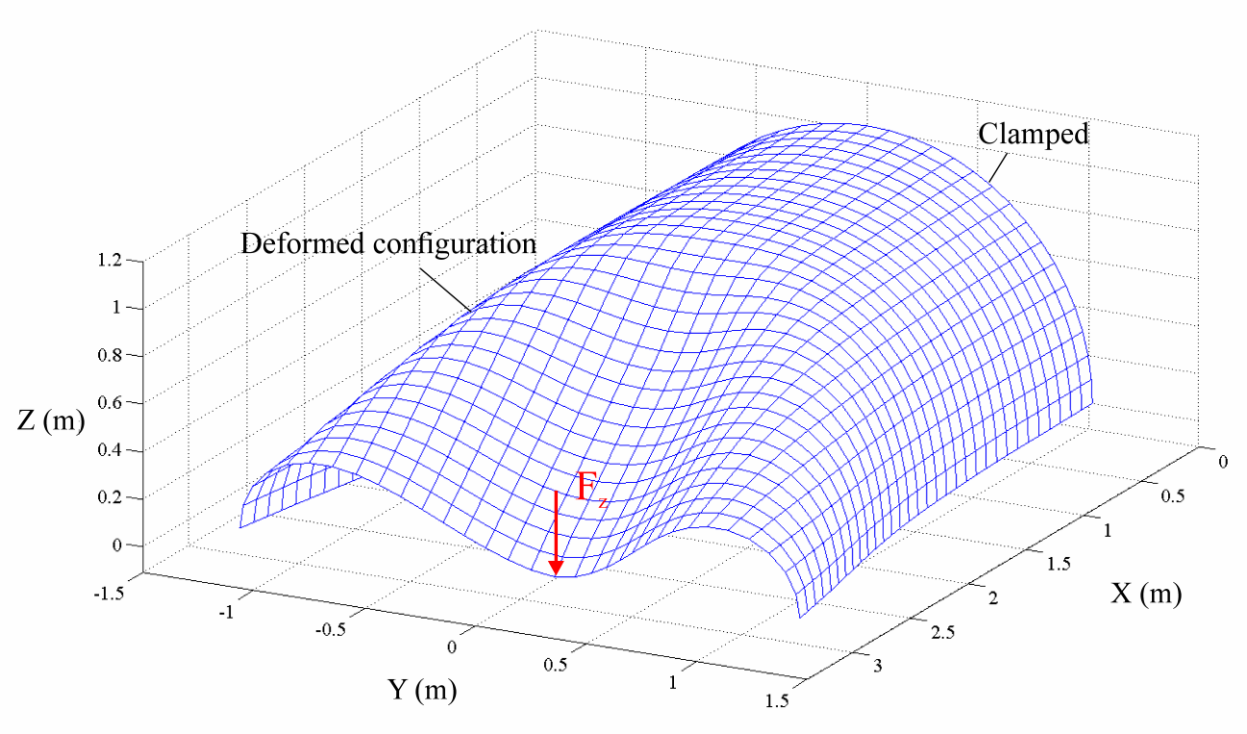

Figure 7. Deformed shape of pinched semi-cylindrical shell

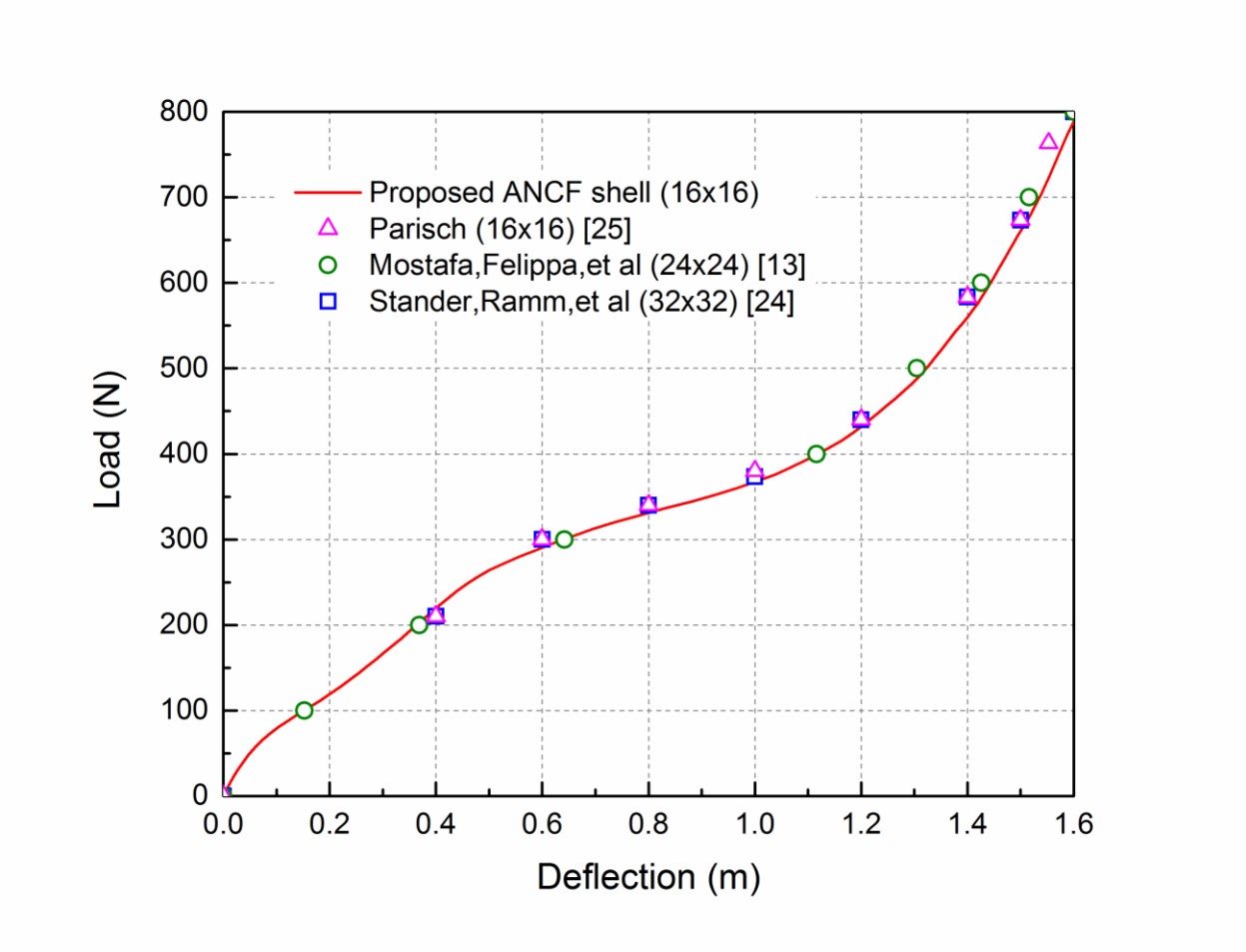

Figure 8. Load-deflection curve of pinched semi-cylindrical shell

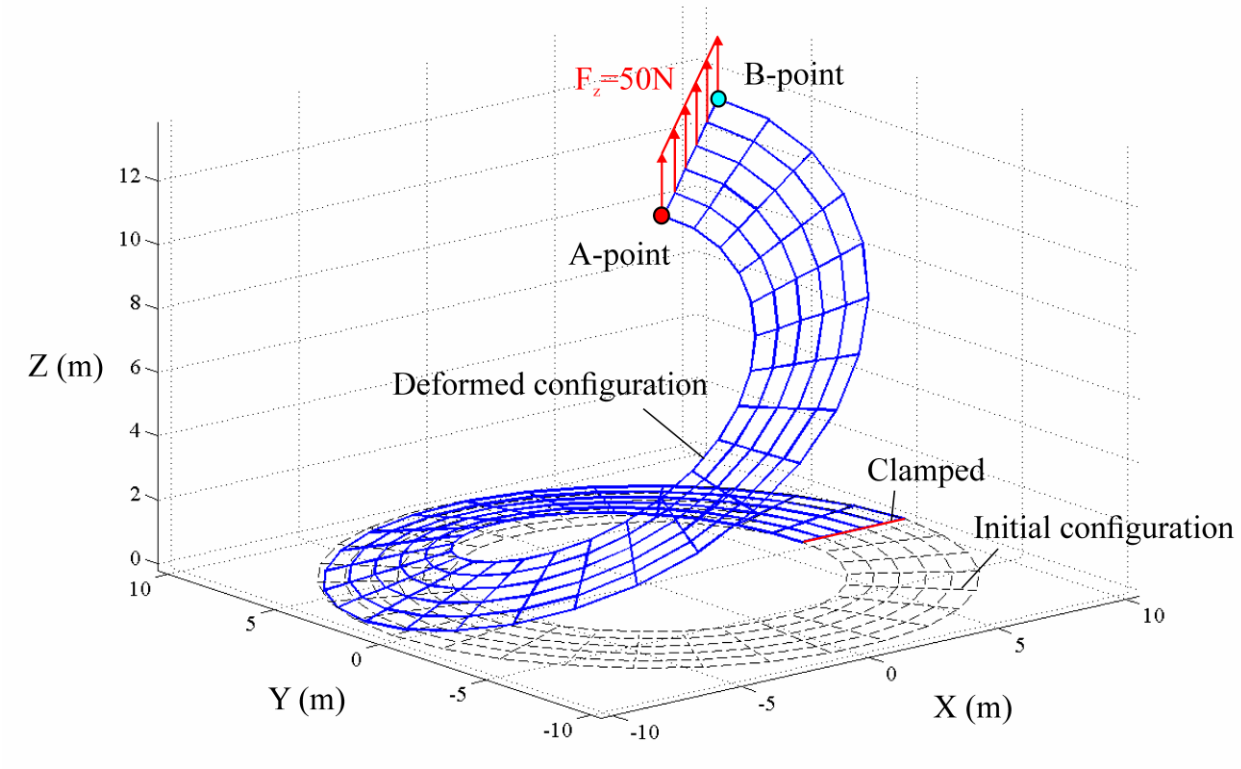

Figure 9. Deformed shape of slit annular plate subjected to lifting force

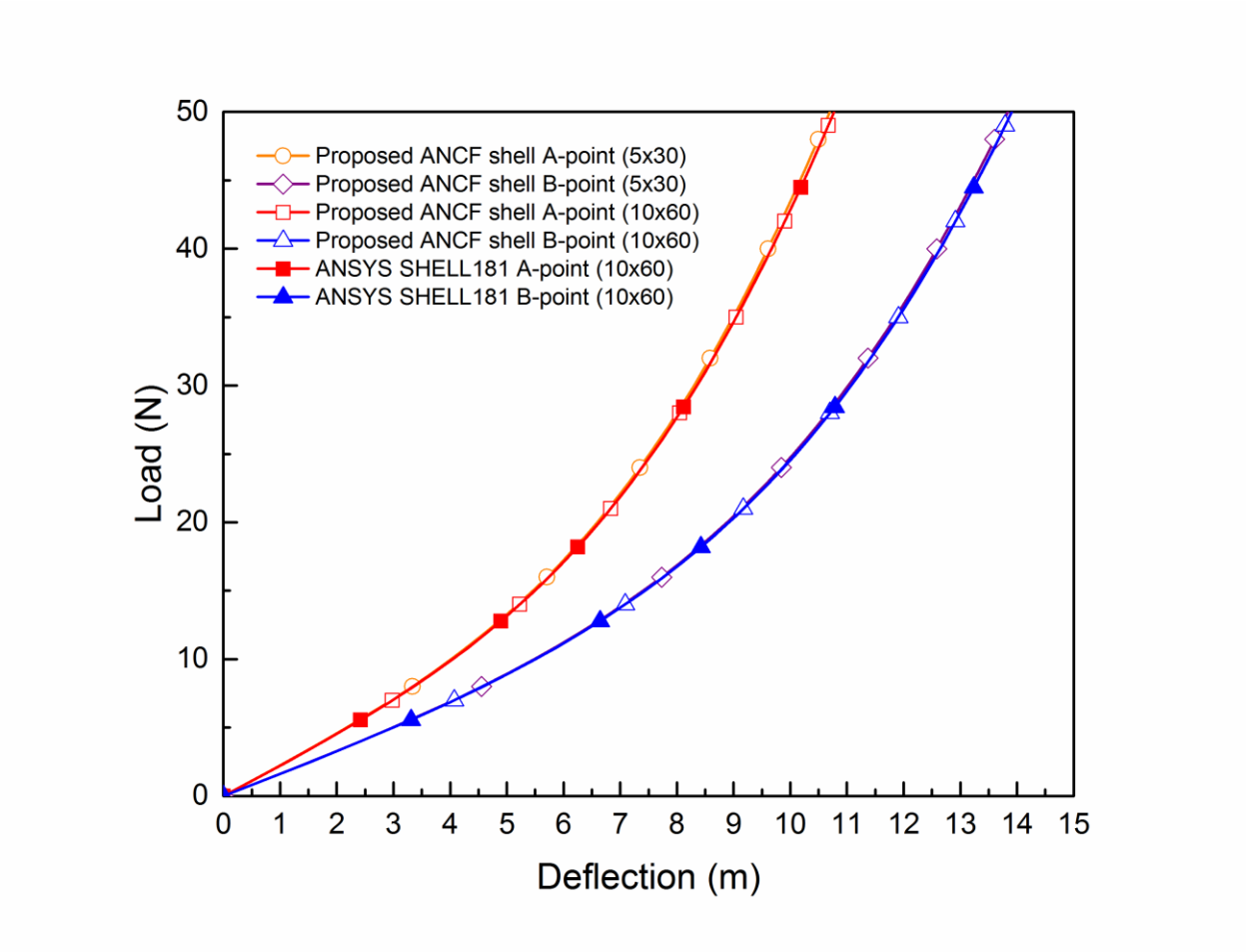

Figure 10. Load-deflection curve of slit annular plate subjected to lifting force

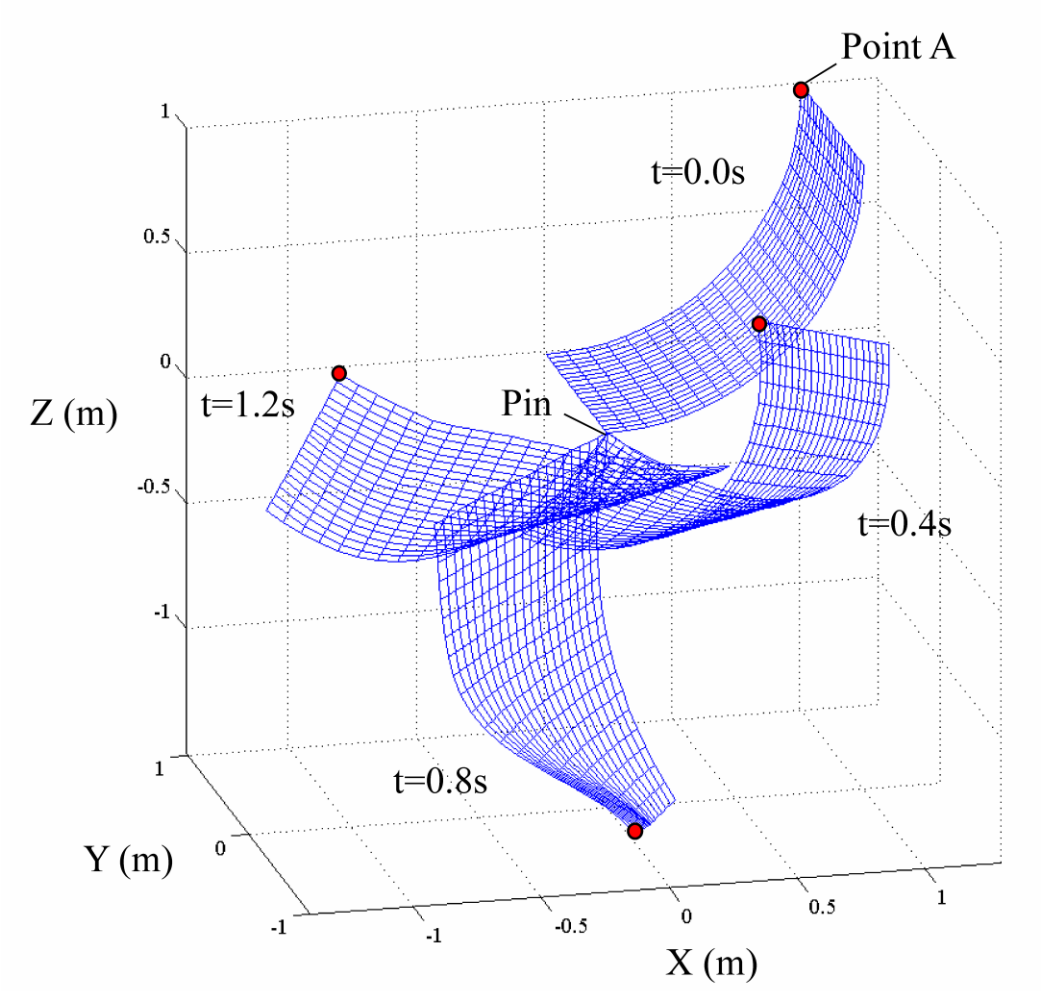

Figure 11. Deformed shapes of quarter-cylindrical shell pendulum

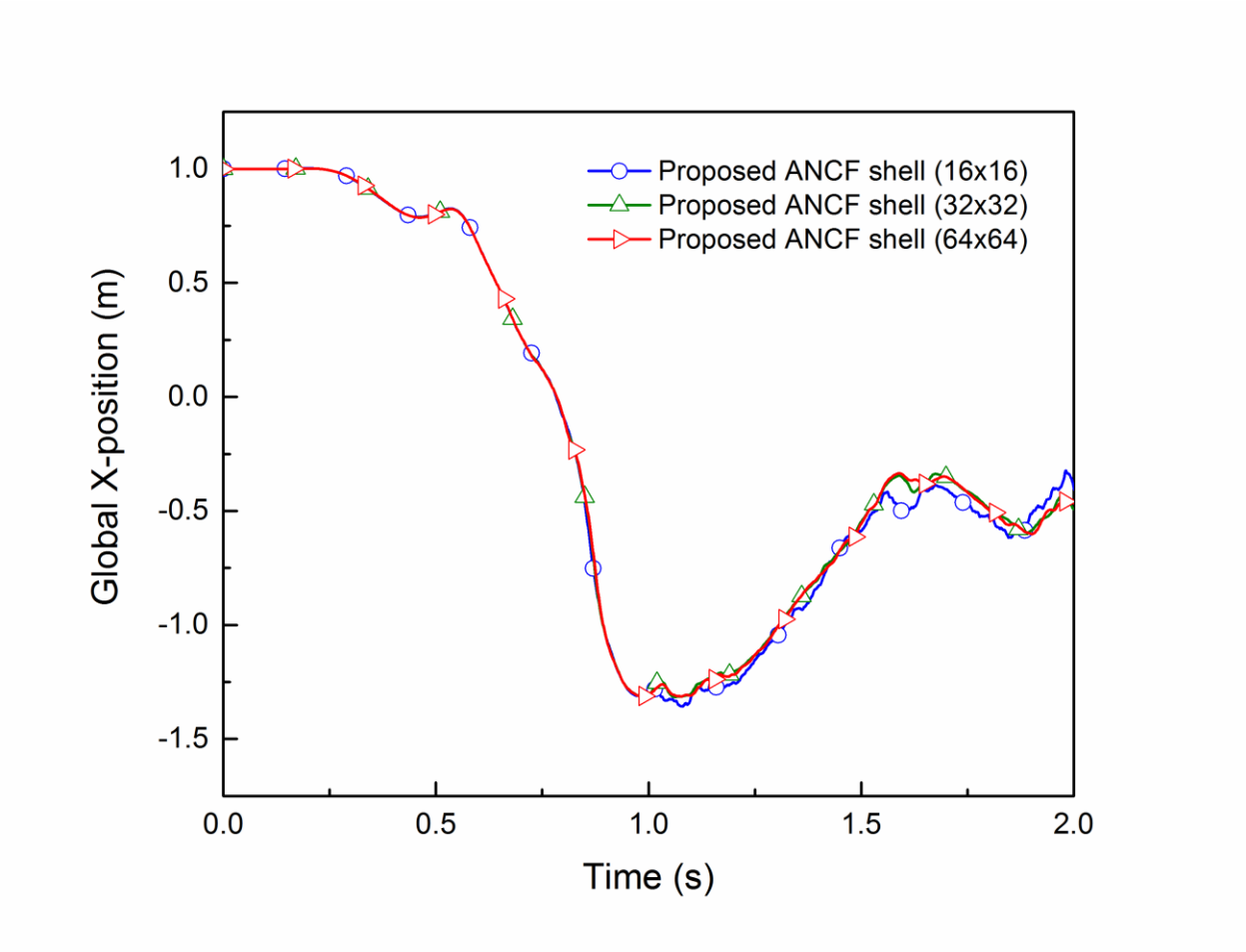

Figure 12. Global X-position at Point A

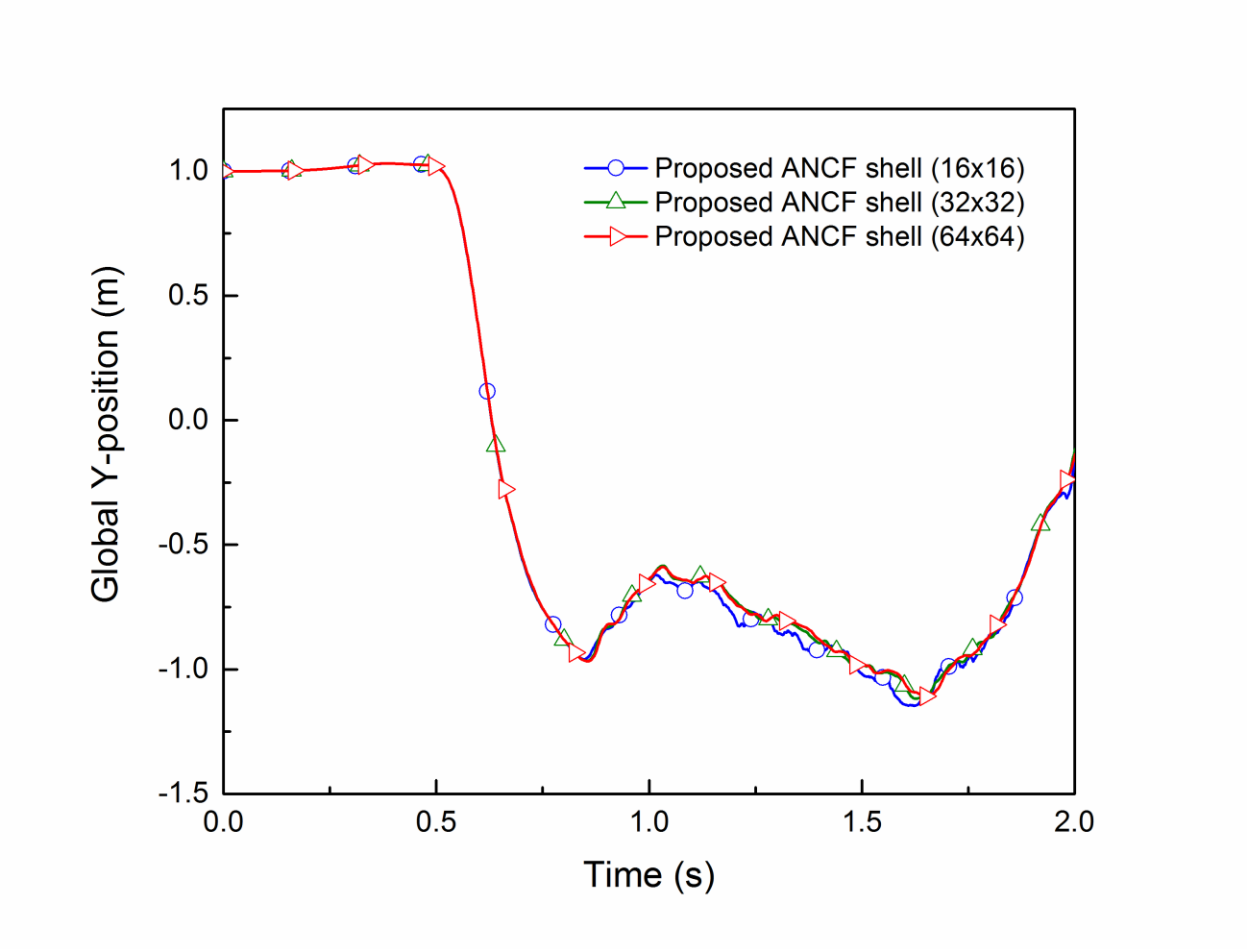

Figure 13. Global Y-position at Point A

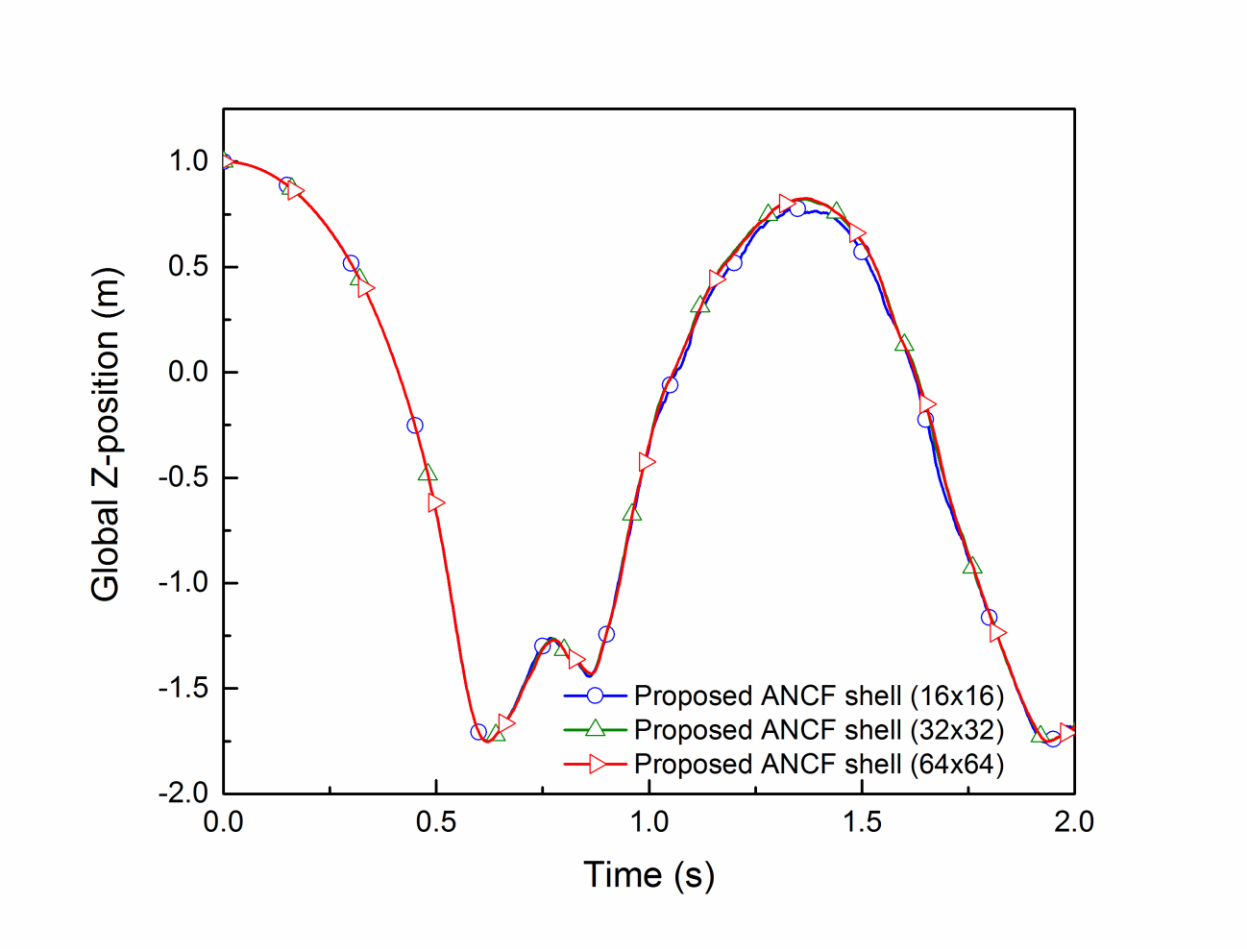

Figure 14. Global Z-position at Point A